# Lower threshold for marsh drowning suggests loss of microtidal marshes regardless of sediment supply

Orencio Duran Vinent[1,2*], Ellen R. Herbert[1,3] & Matthew L. Kirwan[1]

[1] *Virginia Institute of Marine Sciences, College of William and Mary, Gloucester Point, Virginia 23062, USA*

[2] *Department of Ocean Engineering, Texas A&M University, College Station, Texas 77843, USA*

[3] *Ducks Unlimited, Memphis, Tennessee 38129, USA*

∗ *Corresponding author: oduranvinent@tamu.edu*

**Salt marshes are simultaneously among the most valuable and vulnerable ecosystems in the world. We use a simplified formulation for sediment transport across marshes to explain why marshes are most vulnerable to sea level rise (SLR) in microtidal environments. We find inorganic sediment decay length scales with tidal range so that inorganic deposition is very low in the interior of microtidal marshes regardless of the suspended sediment concentration at marsh edge. We also find that drowning of interior marshes eventually leads to a runaway marsh loss due to the approximate scale invariance of inorganic deposition. Thus, organic accretion rather than inorganic accretion is the key factor determining microtidal marsh survival. In fact, because in many locations the rate of SLR is close to or exceeds a theoretical maximum organic accretion rate for tidal salt marshes, our results suggest impending drowning of global microtidal marshes regardless of local sediment supply.**

Salt marshes adapt to sea level rise by accumulating organic matter and by inorganic accretion. The natural limit of these processes defines a threshold rate of SLR beyond which marshes drown. There is a growing consensus that marsh vulnerability to SLR is tied to inorganic sediment availability [1–4], where deposition of inorganic sediment increases with flooding duration, and potentially offsets sea level rise. Indeed, inorganic deposition rates have accelerated over the last century concomitant with sea level rise (SLR) [5,6] and historic

marsh loss has been observed mostly in sediment-poor systems [7,8] and microtidal marshes [9]. Modeled threshold rates of sea level rise for marsh drowning, using simplified point (0-D) models, increase by 2 orders of magnitude as a function of suspended sediment concentration and tidal range [10,11]. However, a contrasting body of work emphasizes the importance of organic matter accumulation in building marsh soils in the face of sea level rise, especially in the sediment deficient estuaries most vulnerable to sea level rise [1,9,12–15]. Total marsh accretion rates are more strongly correlated with the organic fraction of marsh soil than the inorganic fraction [12], organic matter contributes 4 times more soil volume than an equivalent mass of inorganic sediment [14], and organic matter represents the majority of marsh accretion by volume in many Atlantic and Gulf Coast marshes [12–14].

Competing ideas about the relative importance of organic and inorganic accretion likely reflect strong spatial gradients within marshes [16–18]. Inorganic accretion increases with suspended sediment concentration and flooding depth, and decreases with distance to tidal channels, as reported both in the field [19–23] and in models [16–18,23–27]. Organic accretion is influenced by the production and decomposition of plant biomass, both of which vary spatially across marshes in response to flooding depth as well as other factors. Moreover, vegetation itself enhances inorganic sediment deposition so that organic and inorganic contributions are thoroughly intertwined [28,29]. These gradients lead to complex patterns of marsh accretion and submergence that are sometimes difficult to explain. For example, marshes along the Blackwater River (MD, USA) are rapidly submerging despite having a larger sediment supply, characterized by the suspended sediment concentrations measured in channels, than in nearby stable marshland[30,31]. Elsewhere, marshes are submerging despite measured accretion rates that are similar to or exceed sea level rise[2,31,32], which suggests measurements take place mostly along marsh edges, where maximum accretion rates are generally observed.

This complexity leads to the simple question: where in a marsh should organic and inorganic contributions

to marsh accretion be characterized to best evaluate marsh vulnerability to sea level rise? Measurements from high elevation portions of a marsh potentially underestimate future marsh accretion because inorganic accretion rates may accelerate with increased flooding duration [2]. However, if low elevation marshes are also closest to channels, then accretion rates from low elevation portions of the marsh would overestimate accretion to the marsh as a whole, and lead to an underestimation of marsh vulnerability to sea level rise.

A third possibility, suggested by numerical simulations [17], is that marsh drowning is not described by a single threshold but is instead a gradual process where different portions of the marsh platform drown at different rates of SLR. Contrary to this, here we show that runaway marsh drowning can indeed be described by a well defined threshold rate of SLR. Once this threshold is crossed, there is no equilibrium for a marsh platform which then starts to degrade progressively. Successive increments of the rate of SLR only change the rate of marsh loss. This result is based on a new analytical model for inorganic sedimentation and theoretical considerations supported by simulations and field observations. The analytical model predicts spatial gradients in inorganic accretion rates without the need for spatially explicit hydrodynamic and sediment transport models and reproduces the main features of an equilibrium marsh platform.

## Results and Discussion

**Critical depth for marsh recovery.** The current understanding of the onset of marsh loss is that it takes place whenever marsh depth relative to mean high water is higher than a critical value $D_c$ above which marshes are replaced by tidal flats as the more stable morphology [33–35]. Indeed, field data suggests marsh conversion to tidal flats starts at a critical depth $D_c$ around 35% of the tidal range $\delta z$ (corresponding to an average rescaled inundation time $\tau_c = \pi^{-1} \arccos\left(1 - 2D_c/\delta z\right)$ of about 40%, Fig. 1 and Methods) [33–36]. Therefore, a general condition for the onset of marsh drowning is when the relative rate $R$ of sea level rise

exceeds the sum of the organic ($A_o^c$) and inorganic ($A_i^c$) accretion rates evaluated at the critical depth $D_c$ (Fig. 1a). Because of the spatial variation of inorganic deposition, the lowest inorganic accretion rate at the critical depth thus defines the lowest threshold for marsh drowning.

**Exponential decay of the inorganic accretion rate.** In order to derive a general expression for the lowest threshold for marsh drowning we start with a minimal sediment transport model that captures the central physics of the phenomena (see Methods and Supplementary Figs. S1 & S2). Accordingly, we calculate the inorganic accretion rate $A_i$ across a hypothetical marsh platform of depth $D$ using a one-dimensional formulation for the mass conservation of water and inorganic sediments [4,25,26,37–39]. As inorganic sediments in the water column settle on the marsh surface, where erosion is assumed to be negligible [25], $A_i(x, D)$ decays with the distance $x$ from the channel or tidal flat (Fig. 2). The inorganic accretion rate reaches its lowest value at the location furthest away—a distance $L$—from marsh edges (Fig. 2a), defined in the model as the watershed divide (see Methods). This decay can be well approximated by an exponential function (as proposed by [23] and observed by [21]), with decay length $L_c$,

$$A_i(x, D) = A_i(0, D)\mathrm{e}^{-x/L_c}\,, \tag{1}$$

where $A_i(0, D) \propto \rho_i^{-1} C_0 w_f \tau(D)$ is the accretion rate at the channel bank or marsh edge (see Methods for the proportionality factor), $C_0$ is the average suspended sediment concentration at the channel bank or marsh edge during flood, $\rho_i$ is the effective density of inorganic sediments deposited on the marsh, $w_f$ is the effective sediment settling velocity and $\tau(D) = \pi^{-1} \arccos(1 - 2D/\delta z)$ is the rescaled inundation time at marsh depth $D$. Neglecting spatial changes in the effective sediment falling velocity $w_f$, the predicted inorganic accretion rate at the marsh edge $A_i(0, D)$ is mostly controlled by the sediment concentration $C_0$ and the rescaled inundation time, as expected from mass conservation.

The exponential approximation (Eq. 1) is valid everywhere except in the region around the watershed divide, where tidal flow stops and the simulated accretion rates converge to zero (Methods, Fig. 2). In reality,

complex tidal flows may lead to residual accretion rates in the marsh interior (e.g. [20]), in which case the exponential approximation provides an upper limit to evaluate the resiliency of drowning marshes. This is confirmed by a comparison to empirical data. The exponential decay correctly predicts the spatial gradient in inorganic accretion for a wide variety of North American and European salt marshes [19–21,23,40] (Fig. 3 and Supplementary Fig. S3). In particular, empirical accretion rates in the marsh interior are either similar to or lower than the exponential approximation.

**Scaling of the decay length of inorganic sedimentation.** The spatial decay of inorganic accretion—and thus the difference between the upper and lower thresholds for marsh loss in the marsh edge and marsh interior, respectively—is controlled by the decay length $L_c$. This length scales as the ratio of the tidal discharge per unit width and the effective sediment settling velocity $w_f$, in agreement with the scaling of the deposition length in unidirectional turbulent suspensions [41] (Methods). Tidal discharge per unit width scales as $L\delta z/T$ (Methods), where $\delta z$ is the tidal range, $T$ is the tidal period and $L$ is the characteristic length of the local drainage basin. Thus, the decay length has the form

$$L_c = \beta L \delta z/(T w_f)\,, \tag{2}$$

with fitting parameter $\beta \approx 1.5$, in agreement with both numerical simulations and analytical approximations (Methods and Fig. 2b). The scaling of $L_c$ with the tidal range $\delta z$ means that suspended sediments deposit closer to channels (or tidal flats) at lower tidal ranges, whereas they are more homogeneously distributed at higher tidal ranges. This is consistent with the trend observed in field measurements (Fig. 3), in particular the contrast between the almost homogeneous inorganic accretion in the Bay of Fundy, CA [40] ($\delta z = 11$m), and the noticeable decay observed in Phillips Creek, US [23] ($\delta z = 1.4$m).

The scaling of $L_c$ with $L$ in Eq. 2 follows from the approximate scale invariance of tidal flows, i.e. faster flows—and increasing sediment advection—on larger basins [37]. This scale invariance, where sediments are deposited farther away from the channels in large basins as compared to small ones (Fig. 4), has one

important implication: the lowest inorganic accretion rate at the critical depth for marsh conversion to tidal flats, $A_i^c(L) = A_i(L, D_c) = A_i^c(0)\mathrm{e}^{-L/L_c}$, does not depend on drainage basin size $L$ and can be evaluated without the need of spatially-explicit hydrodynamic models [24,25,27,39,42]. Indeed, after substituting the scaling for the decay length we get:

$$A_i^c(L) = A_i^c(0)\mathrm{e}^{-w_f^+/\beta}\,, \tag{3}$$

where $w_f^+ = w_f T/\delta z$ is the rescaled effective falling velocity and $A_i^c(0) \propto \rho_i^{-1} C_0 w_f \tau_c$ is the critical accretion rate at the channel bank or marsh edge (see Methods for the proportionality factor). In what follows, we use the watershed divide as a formal definition of the marsh interior. Furthermore, for simplicity we will refer to $A_{i,i}^c = A_i^c(L)$ and $A_{i,e}^c = A_i^c(0)$ as the critical inorganic accretion rates in the marsh interior and marsh edge, respectively.

**Effect of tidal range on critical marsh accretion.** An important consequence of the physical mechanisms driving sediment redistribution across the marsh platform, as summarized in Eq. 3, is that the predicted critical inorganic accretion rate in the marsh interior $A_{i,i}^c \equiv A_i^c(L)$ strongly depends on the tidal range (Fig. 5). For typical values of the parameters (see Methods), $A_{i,i}^c$ becomes negligible for tidal ranges $\delta z <$ 1m, regardless of the sediment supply (Fig. 5), in stark contrast to the maximum inorganic accretion rate at the marsh edge (Fig. 5a). More generally, for most microtidal marshes ($\delta z < 1.5$m) the predicted critical accretion rate in the marsh interior ($A_{i,i}^c$) is well below the global mean SLR rate of 3.5 mm/yr (Fig. 5b) and organic accretion becomes crucial for marsh survival.

This explains the apparent contradiction of Blackwater marshes (Figs. 5b), where a relatively high sediment supply into the marsh does not prevent drowning [30,31]. With a tidal range $< 0.5$m, inorganic accretion is irrelevant for the vast majority of the marsh platform. Thus, it is enough for the local rate of SLR to be higher than the organic accretion rate to induce widespread drowning (as indeed seems to be the case [43]). The predicted low inorganic deposition in the marsh interior also agrees with the predominantly organic

composition of sediments found in many marshes with tidal range $< 1$m (e.g. Blackwater, MD [43]; Gulf of Mexico [12]).

We obtain predictions for the critical marsh accretion rates at the marsh edge and marsh interior, $A_o^c + A_{i,e}^c$ and $A_o^c + A_{i,i}^c$ respectively, using a theoretical estimation of the maximum contribution of organic accretion for salt marshes [1] ($A_o^c \approx 3$mm/yr). This value is consistent with accretion rate data of Mid-Atlantic US salt marshes and falls within a broader range of direct and indirect estimations of organic accretion rates of marshes elsewhere (Fig. 6 and Methods). For a characteristic value of the average suspended sediment concentration at the channel bank or marsh edge [44], $C_0 = 50\mathrm{g/m^3}$, the predicted range of critical marsh accretion rates is in general agreement with reported values of accretion rates for global marshes [44] (Fig. 7). We expect most data corresponding to healthy marshes to fall below our prediction for interior marshes as by definition healthy marshes have elevations above the critical value for marsh drowning. Note that a more precise comparison with measured rates will require the distance of the measured point to the nearest sediment source and the average suspended sediment concentration at the marsh edge.

**Threshold for marsh drowning.** The critical marsh accretion rate in the marsh interior ($A_o^c + A_{i,i}^c$), in contrast to the much higher rate at the marsh edge, defines the lowest threshold rate of SLR for marsh drowning. The scale invariance of spatial sediment deposition patterns implies that interior marsh loss around the watershed divide will propagate with time, and lead to runaway marsh loss even if the channel network expands, as shown by one-dimensional simulations (Methods, Fig. 8a). In submerging marshes, interior marshes drown and convert to ponds [17,26,32,34,36,45], which tend to expand until they connect to the channel network usually via the formation of a new small channel [32,45], thereby increasing channel density. Although there are more channels (or connected ponds) to potentially redistribute sediments into the marsh platform, the sediment will be deposited closer to the banks as water flow slows down in the now smaller basins, which could explain the lack of impact of increased channel density on marsh accretion rates in

Louisiana [46]. As a result, the drowning threshold will be crossed around the watershed divide of the new system, leading to marsh drowning at smaller scales (Fig. 8a). With time, local marsh failure propagates from large to small scales following the adjustment of the channel network and tidal flows to an increase in open water area, until most of the marsh is lost. This helps explain the self-similar pattern of marsh loss found in rapidly submerging marshes such as in Louisiana and Blackwater, MD (Fig. 8b,c), where drowning begins near the watershed divide and propagates towards the channels [45]. Note that this pattern disappears in the absence of connected ponds when a new stable marsh equilibrium is reached (Fig. 8d).

This drowning mechanism only requires that connected ponds decrease the size of local drainage basins, regardless of whether they deliver sediment to the marsh platform or not. In the best case scenario depicted in Fig. 8a, connected ponds redistribute inorganic sediment as effective as large channels or mud flats, which is not the case in reality. In fact, any decrease in sediment delivered by connected ponds leads to lower inorganic accretion rates on the surrounding marshes, thereby accelerating marsh drowning.

**Vulnerability to sea level rise.** Similarly to the trend of inorganic accretion rates with tidal range (Fig. 5), the predicted threshold rate of SLR for marsh drowning ($A_o^c + A_{i,i}^c$, Fig. 9) shows a fundamental vulnerability for most microtidal marshes ($\delta z < 1.5$m) as inorganic accretion is too low for them to survive current values of SLR rates without organic accretion contribution. Again, this vulnerability is highest for marshes with tidal ranges $<$ 1m, where inorganic accretion in marsh interior is negligible and the threshold SLR rate seems to be completely determined by organic accretion. In fact, because the survival of microtidal marshes ($\delta z < 1.5$m) mostly depends on organic accretion, we should expect widespread drowning once the rate of SLR crosses the threshold defined by the maximum organic accretion rate. While organic accretion is a complex function of several factors, such as plant species, water salinity, flooding frequency, water and soil temperature and composition [8,14], a meta-analysis of field data reveals organic accretion rates are in the range of $3.0 \pm 2$mm/yr (Fig. 6), which happens to be in the range of SLR rates measured on many global marshes:

$3.5 \pm 1.5$mm/yr. Therefore, it seems we currently are at the tipping point for widespread drowning of global microtidal salt marshes regardless of the local inorganic sediment supply (Fig. 9). Indeed, the model correctly predicts the drowning of Blackwater marshes and also suggests marshes in Venice, the Virginia Eastern Shore (e.g. Phillips Creek) and Plum Island, MA, are particularly vulnerable (Fig. 9).

## Conclusion

Although marsh vulnerability has been traditionally tied to inorganic sediment availability, we find consistently low inorganic accretion in the interior of most microtidal marshes ($\lesssim 3.5$mm/yr, about five times lower than existing predictions, e.g. [16,17,26]), where the threshold for marsh drowning is then defined by organic accretion. Crossing this lower threshold in the marsh interior eventually leads to runaway marsh loss induced by the (approximate) scale invariance of sediment deposition. Furthermore, as the current range of SLR rates happens to be very close to the range of organic accretion rates, our result suggests we are at a tipping point for widespread drowning of microtidal salt marshes. We thus provide a mechanistic explanation for the widely observed fragility of microtidal marshes [9] and show this vulnerability is intrinsic and tied to the dominant role of organic accretion. In this context, factors altering biomass productivity, such as eutrophication, elevated $CO_2$ and climate warming[8,9,17,47], could decide the mid-term response of global microtidal marshes.

## Methods

**Critical depth for marsh recovery.** Measurements of inundation times or marsh depth at either the limit of marsh recovery [34,36] or the transition from marshes to tidal flats [33,35,48] are consistent with a rescaled inundation time $\tau_c = 0.4$, and thus a rescaled critical depth $D_c/\delta z = 0.35 = 0.5(1 - \cos(\pi\tau_c))$ for marsh drowning. The reported data is: $D_c/\delta z = 0.38 \pm 0.05$ for Plum Island, MA [36]; $D_c/\delta z = 0.35 \pm 0.07$ for Venice, Italy [35,48]; $D_c/\delta z = 0.23 \pm 0.06$ for regions of the Scheldt estuary, NL [33]; $\tau_c = 0.42 \pm 0.05$ for

Hallegat and Paulina marshes, NL [34].

**Minimal model of inorganic sedimentation.** We consider one-dimensional depth-integrated mass conservation equations for tidal water discharge per unit width $Q(x,t)$ and depth-averaged suspended sediment concentration $C(x,t)$ over a flat marsh surface with elevation $Z$ relative to mean sea level (MSL). Assuming, (i) a quasi-static tidal propagation with average water elevation (relative to MSL) $\eta(t) = \delta z/2\cos(2\pi t/T)$ with tidal range $\delta z$ and period $T$, (ii) no net sediment erosion, and (iii) negligible lateral diffusion, the conservation of suspended sediments reads [4,25,26,37–39]:

$$\partial_t(HC) + \partial_x(QC) \;\; = \;\; -w_f C \tag{4}$$

where $x$ is the flow direction, $H(t) = \eta(t) - Z$ is water depth and $w_f$ is an effective sediment falling velocity. $Q$ is obtained from the continuity equation $\partial_x Q = -\partial_t \eta$ assuming no water flux ($Q(L,t) = 0$) at the watershed divide $x = L$: $Q(x,t) = \partial_t \eta\,(L-x) = -\delta z L T^{-1}\pi \sin(2\pi t/T)\,(1 - x/L)$. $Q$ thus scales as $\delta z L/T$. Equation 4 is solved during positive water depths ($H(t) > 0$) using two boundary conditions, a constant suspended sediment concentration ($C(0,t) = C_0$) at the channel bank ($x = 0$) during flood ($t < 0$) and no sediment crossing the watershed divide ($C(L,t) = 0$) during ebb ($t > 0$). Using rescaled time ($t^+ = t/T$) and distance ($x^+ = x/L$), the rescaled concentration $C(x^+,t^+)/C_0$ for a given marsh elevation $Z$ is only function of one dimensionless number: the rescaled effective falling velocity $w_f^+ = w_f T/\delta z$ (Fig. S1).

**Analytical approximation.** A further simplification is obtained by averaging Eq. 4 over times of positive water depths in a tidal cycle,

$$\partial_x \overline{QC} = -w_f \overline{C} \tag{5}$$

where the bar denotes averaged quantities. Using the numerical solution of Eq. 4, we find that the mean sediment flux per unit width ($\overline{QC}$) decreases linearly with the mean suspended sediment concentration ($\overline{C}$) in the range $x/L \lesssim 0.6$, and can be approximated as $\overline{QC} \approx \beta \delta z L T^{-1}\overline{C} + \beta_2$, with fitting constants $\beta = 1.5$

and $\beta_2$ (Fig. S2). Thus, Eq. 5 can be approximated as

$$\beta\, L\partial_x \overline{C} = -w_f^+ \overline{C} \tag{6}$$

with boundary condition $\overline{C}(0) = C_0 r(w_f^+)$, where the fitting function

$$r(w_f^+) = \left[1 + (1 + w_f^+)^{-1}\right]/2 \tag{7}$$

represents the effect of sediment inertia in the temporal decrease of suspended sediments during ebb flows.

**Mean suspended sediment concentration and decay length.** The solution of Eq. 6 is the exponential

$$\overline{C}(x) = C_0 r(w_f^+) \exp\left(-x/L_c\right) \tag{8}$$

with decay length $L_c = \beta L/w_f^+ = \beta L\delta z/(Tw_f)$.

**Scaling of decay length in turbulent suspensions vs. tidal flows.** In unidirectional turbulent suspensions [41] the decay or deposition length scales as $L_c \propto HU/w_f \propto Q/w_f$, where $H$ is the flow depth, $U$ is the (constant) flow velocity, $w_f$ is the falling velocity and $Q \propto UH$ is the water discharge per unit width. In tidal flows, the decay length has the same scaling with the ratio $Q/w_f$ but now $Q \propto \delta z L/T$ and thus $L_c \propto Q/w_f \propto L\delta z/(Tw_f)$.

**Inorganic accretion rate.** The inorganic accretion rate averaged over a tidal cycle for a marsh depth $D = \delta z/2 - Z$ (relative to mean high water level (MHW)) is defined as $A_i(x, D) = \rho_i^{-1} w_f\, \tau(D)\, \overline{C}(x)$, where $\rho_i$ is the density of inorganic sediments deposited in the marsh and $\tau(D) = \pi^{-1} \arccos\left(1 - 2D/\delta z\right)$ is the rescaled inundation time (fraction of time below water). Using Eq. 8, $A_i(x, D)$ can be approximated as

$$A_i(x, D) \approx A_i(0, D) \exp\left(-x/L_c\right) \tag{9}$$

where the accretion rate at the marsh edge is $A_i(0, D) = \rho_i^{-1} C_0 w_f\, r(w_f^+)\tau(D)$.

**Inorganic accretion rate at $D_c$.** At the critical depth ($D_c = 0.35\delta z$) for marsh drowning, the critical inorganic accretion rates $A_i^c(x) = A_i(x, D_c)$ at the marsh edge ($A_{i,e}^c$) and marsh interior ($A_{i,i}^c$) become:

$$A_{i,e}^c = A_i^c(0) = \rho_i^{-1} C_0 w_f \, r(w_f^+) \tau_c \tag{10}$$

$$A_{i,i}^c = A_i^c(L) = A_{i,e}^c \exp\left(-w_f^+/\beta\right). \tag{11}$$

where $\tau_c = \tau(D_c) \approx 0.4$ is the rescaled inundation time at the critical depth and the function $r(w_f^+)$ is given in Eq. 7.

**Simplified one-dimensional model of marsh drowning.** We assume three possible responses of the bed or marsh elevation $Z(x,t)$ to sea level rise depending on the critical elevation $Z_c$ and an arbitrary lower elevation $Z_t$:

$$\partial_t Z = \begin{cases} A_i(x, Z, t) + A_o - R & \text{for } Z > Z_c \\ -R & \text{for } Z_t < Z < Z_c \\ 0 & \text{for } Z < Z_t \end{cases} \tag{12}$$

Above the critical elevation $Z_c$, marshes are widespread and the elevation changes at the rate $A_i(x, Z, t) + A_o - R$, where we substitute marsh depth ($D$) for marsh elevation ($Z = \delta/2 - D$). We assume for simplicity a constant organic accretion rate $A_o$. Using Eq. 9 for the inorganic accretion rate, substituting the rescaled decay length $L_c/L$, and approximating $\pi^{-1}\arccos(x)$ by $(1-x)/2$ in the rescaled inundation time $\tau$, we get:

$$A_i(x, Z, t) \approx \frac{C_0 w_f}{\rho_i} \, r(w_f^+) \, \left[\frac{1}{2} - \frac{Z(x,t)}{\delta z}\right] \exp\left[-\ell(x,t)\, w_f^+/\beta\right], \tag{13}$$

where the function $\ell(x,t) \in [0,1]$ is defined as the distance from the edge of a given channel rescaled such that $\ell = 1$ at the corresponding watershed divide (e.g. $\ell(x) = x/L$ if the marsh edge is at $x = 0$ and the watershed divide at $x = L$). The watershed divide is defined as the midpoint between neighboring channels (or connected ponds.)

Below $Z_c$, but above $Z_t$, marshes starts to degrade forming ponds ($A_o = 0$). We assume these ponds are isolated with no net inorganic accretion ($A_i = 0$), and thus get deeper with SLR at a rate: $\partial_t Z = -R$.

Ponds deeper than $Z_t$ are assumed to connect to the channel network and change the geometry of the drainage basin. For simplicity, we assume ponds keep a constant depth afterwards (lower than $Z_t$) and become a new source of both tidal water and inorganic sediment with concentration $C_0$. Note that this is an ideal best-case scenario, as in reality connected ponds do not deliver much sediment to the marsh platform, which would decrease inorganic accretion rates in marshes around connected ponds and thus increase their drowning rate.

We numerically integrate Eqs. 12 and 13, for interior-marsh drowning scenarios ($R \geq A_o + A^c_{i,i}$), starting with a marsh platform of arbitrary elevation and length, limited by tidal channels at both sides (Fig. 8). As new ponds connect to the channel network ($Z < Z_t$), we update the term $\ell(x,t)$ to reflect the positions of the new marsh edges (defined by the condition $Z = Z_t$), and corresponding watershed divides.

**Parameters for figures and data comparison.** We use $w_f = 10^{-4}$ m/s, which is within commonly reported ranges[3,20,49] and $\rho_i = 2$ g/cm$^3$, obtained from a meta-analysis of bulk density measurements in global marshes[1]. Parameters for Fig. 8: $\delta z = 1$m, $C_0 = 50$g/m$^3$, $R = 7$mm/yr, $A_0 = 3$mm/yr, $Z_c = 0.15$m (critical elevation for marsh drowning) and $Z_t = 0.1$m (elevation for pond connection to channel network).

**Organic accretion rates** For some locations in USA (North and South Carolina, Mid-Atlantic and Texas & Florida) we used the data compilation from [12], which reports the total accretion rate range (min and max values) and the slope (cm$^3$g$^{-1}$) of the linear regression between organic mass accretion rates (defined as the dependent variable, g cm$^{-3}$yr$^{-1}$) and total accretion rates (defined as the independent variable, cm yr$^{-1}$). We then obtain min and max values for organic mass accretion rates and convert them from mass to volume using an effective density of deposited organic matter: $\rho_o = 0.085$ g/cm$^3$, obtained from a meta-analysis of

bulk density measurements in global marshes [1]. For Rhodes Island, US, we use reported values of organic mass accretion rates [50] converted to volume using $\rho_o$. We did the same for some marshes in Louisiana, US [46]. We also used reported values of organic accretion rates (mm/yr) for some locations in the Scheldt estuary, NL [49]. For Venice, we estimate organic accretion rates from reported total marsh accretion rates [51], using the average bulk density $\approx 1$ g/cm$^3$ [29] and the effective values for the density of organic and inorganic deposited sediments $\rho_i = 2$ g/cm$^3$ and $\rho_o = 0.085$ g/cm$^3$ respectively [1]. The organic accretion rate data is shown in Fig. 6.


1. Morris, J. T. *et al.* Contributions of organic and inorganic matter to sediment volume and accretion in tidal wetlands at steady state: Sediment bulk density and ignition loss. *Earth's Future* **4**, 110–121 (2016).

2. Kirwan, M. L., Temmerman, S., Skeehan, E. E., Guntenspergen, G. R. & Fagherazzi, S. Overestimation of marsh vulnerability to sea level rise. *Nature Climate Change* **6**, 253–260 (2016).

3. Marani, M., D'Alpaos, A., Lanzoni, S., Carniello, L. & Rinaldo, A. Biologically-controlled multiple equilibria of tidal landforms and the fate of the Venice lagoon. *Geophysical Research Letters* **34** (2007).

4. Fagherazzi, S. *et al.* Numerical models of salt marsh evolution: Ecological, geormorphic, and climatic factors. *Reviews of Geophysics* 1–28 (2012).

5. Kolker, A. S., Kirwan, M. L., Goodbred, S. L. & Cochran, J. K. Global climate changes recorded in coastal wetland sediments: Empirical observations linked to theoretical predictions. *Geophysical Research Letters* **37** (2010).

6. Hill, T. D. & Anisfeld, S. C. Coastal wetland response to sea level rise in Connecticut and New York. *Estuarine, Coastal and Shelf Science* **163**, 185–193 (2015).

7. Day, J. *et al.* Sustainability of Mediterranean Deltaic and Lagoon Wetlands with Sea-Level Rise: The Importance of River Input. *Estuaries and Coasts* **34**, 483–493 (2011).

8. Kirwan, M. L. & Megonigal, J. P. Tidal wetland stability in the face of human impacts and sea-level rise. *Nature* **504**, 53–60 (2013).

9. Kearney, M. S. Microtidal Marshes: Can These Widespread and Fragile Marshes Survive Increasing ClimateSea Level Variability and Human Action? *Journal of Coastal Research* **32**, 686 (2016).

10. D'Alpaos, A., Mudd, S. M. & Carniello, L. Dynamic response of marshes to perturbations in suspended sediment concentrations and rates of relative sea level rise. *Journal of Geophysical Research: Earth Surface* **116** (2011).

11. Kirwan, M. L. *et al.* Limits on the adaptability of coastal marshes to rising sea level. *Geophysical Research Letters* **37**, n/a–n/a (2010).

12. Turner, R. E., Swenson, E. M. & Milan, C. S. Organic and Inorganic Contributions to Vertical Accretion in Salt Marsh Sediments. In *Concepts and Controversies in Tidal Marsh Ecology*, 583–595 (Springer, Dordrecht, 2002).

13. Nyman, J. A., Walters, R. J., Delaune, R. D. & Patrick, W. H. Marsh vertical accretion via vegetative growth. *Estuarine, Coastal and Shelf Science* **69**, 370–380 (2006).

14. Neubauer, S. C. Contributions of mineral and organic components to tidal freshwater marsh accretion. *Estuarine, Coastal and Shelf Science* **78**, 78–88 (2008).

15. Kirwan, M. L. & Guntenspergen, G. R. Feedbacks between inundation, root production, and shoot growth in a rapidly submerging brackish marsh. *Journal of Ecology* **100**, 764–770 (2012).

16. D'Alpaos, A. The mutual influence of biotic and abiotic components on the long-term ecomorphodynamic evolution of salt-marsh ecosystems. *Geomorphology* **126**, 269–278 (2011).

17. Ratliff, K. M., Braswell, A. E. & Marani, M. Spatial response of coastal marshes to increased atmospheric $CO_2$. *Proceedings of the National Academy of Sciences* 201516286 (2015).

18. DAlpaos, A. & Marani, M. Reading the signatures of biologicgeomorphic feedbacks in salt-marsh landscapes. *Advances in Water Resources* **93, Part B**, 265–275 (2016).

19. French, J. R. & Spencer, T. Dynamics of sedimentation in a tide-dominated backbarrier salt marsh, Norfolk, UK. *Marine Geology* **110**, 315–331 (1993).

20. Christiansen, T., Wiberg, P. & Milligan, T. Flow and Sediment Transport on a Tidal Salt Marsh Surface. *Estuarine, Coastal and Shelf Science* **50**, 315–331 (2000).

21. Temmerman, S., Govers, G., Wartel, S. & Meire, P. Spatial and temporal factors controlling short-term sedimentation in a salt and freshwater tidal marsh, Scheldt estuary, Belgium, SW Netherlands. *Earth Surface Processes and Landforms* **28**, 739–755 (2003).

22. Reed, D. J. The response of coastal marshes to sea-level rise: Survival or submergence? *Earth Surface Processes and Landforms* **20**, 39–48 (1995).

23. Fagherazzi, S. *et al.* Fluxes of water, sediments, and biogeochemical compounds in salt marshes. *Ecological Processes* **2**, 3 (2013).

24. Temmerman, S. *et al.* Impact of vegetation on flow routing and sedimentation patterns: Three-dimensional modeling for a tidal marsh. *Journal of Geophysical Research: Earth Surface* **110**, n/a–n/a (2005).

25. D'Alpaos, A., Lanzoni, S., Marani, M. & Rinaldo, A. Landscape evolution in tidal embayments: Modeling the interplay of erosion, sedimentation, and vegetation dynamics. *Journal of Geophysical Research: Earth Surface* **112**, F01008 (2007).

26. Da Lio Cristina, D'Alpaos Andrea & Marani Marco. The secret gardener: vegetation and the emergence of biogeomorphic patterns in tidal environments. *Philosophical Transactions of the Royal Society A: Mathematical, Physical and Engineering Sciences* **371**, 20120367 (2013).

27. Belliard, J. P., Di Marco, N., Carniello, L. & Toffolon, M. Sediment and vegetation spatial dynamics facing sea-level rise in microtidal salt marshes: Insights from an ecogeomorphic model. *Advances in Water Resources* **93**, 249–264 (2016).

28. Mudd, S. M., D'Alpaos, A. & Morris, J. T. How does vegetation affect sedimentation on tidal marshes? Investigating particle capture and hydrodynamic controls on biologically mediated sedimentation. *Journal of Geophysical Research* **115** (2010).

29. Roner, M. *et al.* Spatial variation of salt-marsh organic and inorganic deposition and organic carbon accumulation: Inferences from the Venice lagoon, Italy. *Advances in Water Resources* **93, Part B**, 276–287 (2016).

30. Ganju, N. K. *et al.* Sediment transport-based metrics of wetland stability: Sediment Metrics of Wetland Stability. *Geophysical Research Letters* **42**, 7992–8000 (2015).

31. Ganju, N. K. *et al.* Spatially integrative metrics reveal hidden vulnerability of microtidal salt marshes. *Nature Communications* **8** (2017).

32. Mariotti, G. Revisiting salt marsh resilience to sea level rise: Are ponds responsible for permanent land loss? *Journal of Geophysical Research: Earth Surface* **121**, 1391–1407 (2016).

362 33. Wang, C. & Temmerman, S. Does biogeomorphic feedback lead to abrupt shifts between alternative
363 landscape states?: An empirical study on intertidal flats and marshes. *Journal of Geophysical Research:*
364 *Earth Surface* **118**, 229–240 (2013).

365 34. van Belzen, J. *et al.* Vegetation recovery in tidal marshes reveals critical slowing down under increased
366 inundation. *Nature Communications* **8**, 15811 (2017).

367 35. Defina, a., Carniello, L., Fagherazzi, S. & D'Alpaos, L. Self-organization of shallow basins in tidal
368 flats and salt marshes. *Journal of Geophysical Research* **112**, F03001–F03001 (2007).

369 36. Wilson, C. A. *et al.* Saltmarsh pool and tidal creek morphodynamics: Dynamic equilibrium of northern
370 latitude saltmarshes? *Geomorphology* **213**, 99–115 (2014).

371 37. Rinaldo, A., Fagherazzi, S., Lanzoni, S., Marani, M. & Dietrich, W. E. Tidal networks 2. Watershed
372 delineation and comparative network morphology. *Water Resources Research* **35**, 3905–3917 (1999).

373 38. Carniello, L., Defina, A. & DAlpaos, L. Modeling sand-mud transport induced by tidal currents and
374 wind waves in shallow microtidal basins: Application to the Venice Lagoon (Italy). *Estuarine, Coastal*
375 *and Shelf Science* **102-103**, 105–115 (2012).

376 39. Marani, M., Lio, C. D. & DAlpaos, A. Vegetation engineers marsh morphology through multiple
377 competing stable states. *Proceedings of the National Academy of Sciences* **110**, 3259–3263 (2013).

378 40. van Proosdij, D., Davidson-Arnott, R. G. & Ollerhead, J. Controls on spatial patterns of sediment
379 deposition across a macro-tidal salt marsh surface over single tidal cycles. *Estuarine, Coastal and Shelf*
380 *Science* **69**, 64–86 (2006).

41. Claudin, P., Charru, F. & Andreotti, B. Transport relaxation time and length scales in turbulent suspensions. *Journal of Fluid Mechanics* **671**, 491–506 (2011).

42. Belliard, J.-P., Toffolon, M., Carniello, L. & D'Alpaos, A. An ecogeomorphic model of tidal channel initiation and elaboration in progressive marsh accretional contexts. *Journal of Geophysical Research: Earth Surface* **120**, 1040–1064 (2015).

43. Stevenson, J. C., Kearney, M. S. & Pendleton, E. C. Sedimentation and erosion in a Chesapeake Bay brackish marsh system. *Marine Geology* **67**, 213–235 (1985).

44. French, J. Tidal marsh sedimentation and resilience to environmental change: Exploratory modelling of tidal, sea-level and sediment supply forcing in predominantly allochthonous systems. *Marine Geology* **235**, 119–136 (2006).

45. Schepers, L., Kirwan, M., Guntenspergen, G. & Temmerman, S. Spatio-temporal development of vegetation die-off in a submerging coastal marsh: Spatio-temporal marsh die-off. *Limnology and Oceanography* **62**, 137–150 (2017).

46. DeLaune, R. D., Whitcomb, J. H., Patrick, W. H., Pardue, J. H. & Pezeshki, S. R. Accretion and canal impacts in a rapidly subsiding wetland. I. 137 Cs and 210 Pb techniques. *Estuaries and Coasts* **12**, 247–259 (1989).

47. Reef, R. *et al.* The effects of elevated $CO_2$ and eutrophication on surface elevation gain in a European salt marsh. *Global Change Biology* **23**, 881–890 (2017).

48. Fagherazzi, S., Carniello, L., D'Alpaos, L. & Defina, A. Critical bifurcation of shallow microtidal landforms in tidal flats and salt marshes. *Proceedings of the National Academy of Sciences of the United States of America* **103**, 8337–41 (2006).

49. Temmerman, S., Govers, G., Wartel, S. & Meire, P. Modelling estuarine variations in tidal marsh sedimentation: response to changing sea level and suspended sediment concentrations. *Marine Geology* **212**, 1–19 (2004).

50. Bricker-Urso, S., Nixon, S. W., Cochran, J. K., Hirschberg, D. J. & Hunt, C. Accretion rates and sediment accumulation in Rhode Island salt marshes. *Estuaries* **12**, 300–317 (1989).

51. Bellucci, L. *et al.* 210pb and 137cs as chronometers for salt marsh accretion in the Venice Lagoon links to flooding frequency and climate change. *Journal of Environmental Radioactivity* **97**, 85–102 (2007).

52. Joye, S. B. Long-term water quality monitoring in the altamaha, doboy and sapelo sounds and the duplin river near sapelo island, georgia from may 2001 to august 2009. *Georgia Coastal Ecosystems LTER Project, University of Georgia, LTER Network (doi:10.6073/pasta/964b638bc904b8a4eca4605f682b9c64)* (2009).

53. Blum, L., Christian, R., Brinson, M. & Willis, P. Surface elevation data for the upper phillips creek marsh at the virginia coast reserve 1998-2016. *Virginia Coast Reserve Long-Term Ecological Research Project Data Publication knb-lter-vcr.148.26 (doi:10.6073/pasta/d2418addc6e102fe300fbc26149b5dcc)* (2016).

54. Loomis, M. J. & Craft, C. B. Carbon Sequestration and Nutrient (Nitrogen, Phosphorus) Accumulation in River-Dominated Tidal Marshes, Georgia, USA. *Soil Science Society of America Journal* **74**, 1028 (2010).

**Acknowledgements** Put acknowledgements here.

**Competing Interests** The authors declare that they have no competing financial interests.

422 **Correspondence** Correspondence and requests for materials should be addressed to A.B.C. (email: myaddress@nowhere.edu).

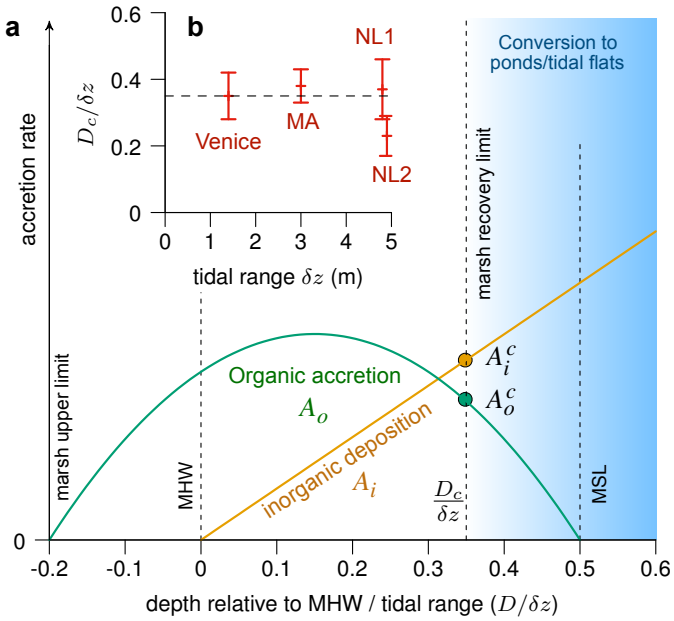


Figure 1: **Critical depth for marsh recovery.** (**a**) Sketch of the organic ($A_o$) and inorganic ($A_i$) accretion rates on a marsh platform as function of the water depth ($D$) relative to mean high water level (MHW) and rescaled by tidal range $\delta z$. Accretion rates ($A_i^c$ and $A_o^c$) at the critical depth for marsh recovery ($D_c$) determine the marsh response to sea level rise. (**b**) Reported measurements of critical depths for Plum Island, MA (MA) [36]; Venice, Italy [35,48]; regions of the Scheldt estuary, NL (NL2) [33]; and in Hallegat and Paulina marshes, NL (NL1) [34].

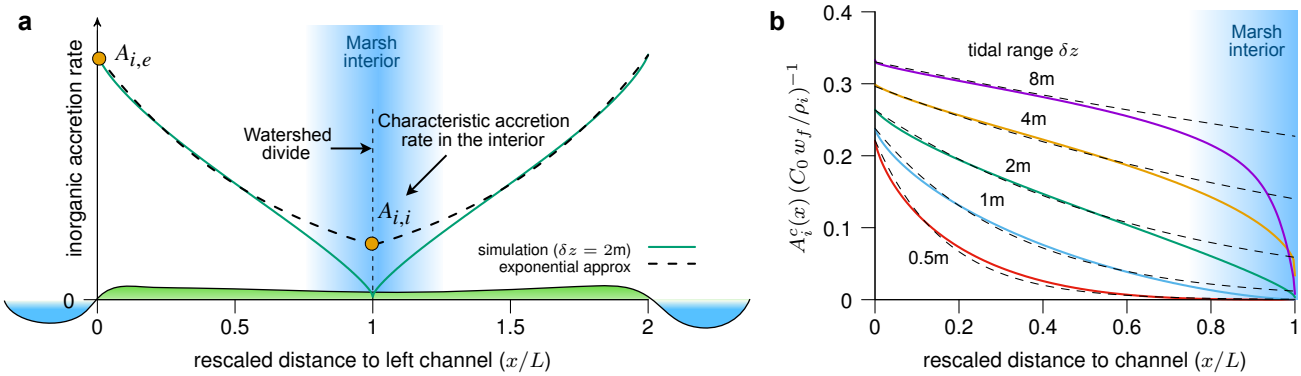


Figure 2: **Spatial decay of the inorganic accretion rate and scaling with tidal range.** (**a**) Simulation and exponential approximation of the decay of the inorganic accretion rate $A_i$ with the rescaled distance from channel $x/L$, where $L$ is the length of the drainage basin. $A_{i,e}$ is the accretion rate at the marsh edge and $A_{i,i}$ is the characteristic accretion rate in the marsh interior. (**b**) Simulated inorganic accretion rate $A_i^c(x)$ at the critical depth $D_c$ (solid lines), rescaled by $C_0 w_f/\rho_i$, for varying tidal range $\delta z$. $C_0$ is the average suspended sediment concentration at the channel bank or marsh edge during flood, $\rho_i$ is the effective density of inorganic sediments deposited on the marsh and $w_f$ is the effective sediment settling velocity. Dashed lines show the exponential approximation with a decay length $L_c$ given by Eq. 2.

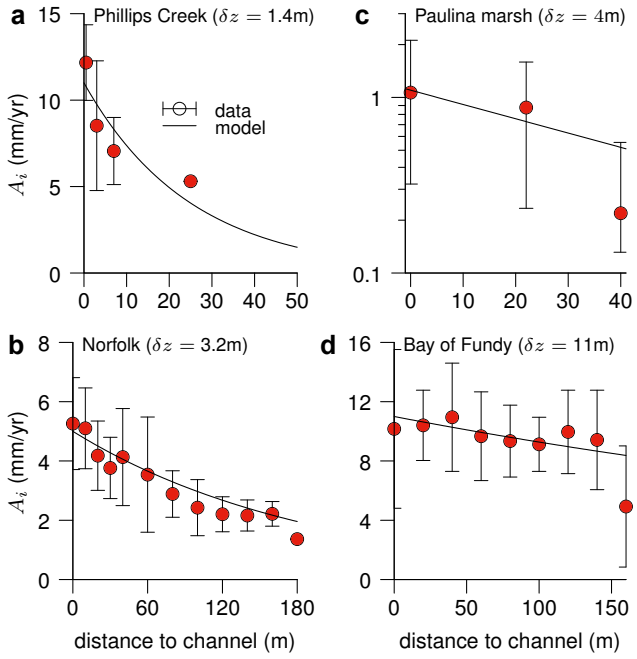


Figure 3: **Validation of the exponential decay of inorganic deposition.** Proposed exponential decay $A_i(0)\exp(-x/L_c)$ compared to field data using the decay length obtained from simulations $L_c = 1.5L\delta z/(Tw_f)$, where $\delta z$ is the tidal range, $T$ is tidal period and $w_f$ is the effective sediment falling velocity. Accretion rates at the channel $A_i(0)$ were fitted to data, $L$ is taken as the maximum distance to channel reported in the data and we use $w_f = 10^{-4}$m/s. Mass accretion rate data was converted to volume accretion rates by dividing by the effective density of inorganic sediments deposited in the marsh $\rho_i \approx 2$g/cm$^3$ [1]. Data sources: (**a**) Phillips Creek, VA[23], (**b**) Norfolk, UK[19], (**c**) Paulina marsh, NL[21] (**d**) Bay of Fundy, CA[40].

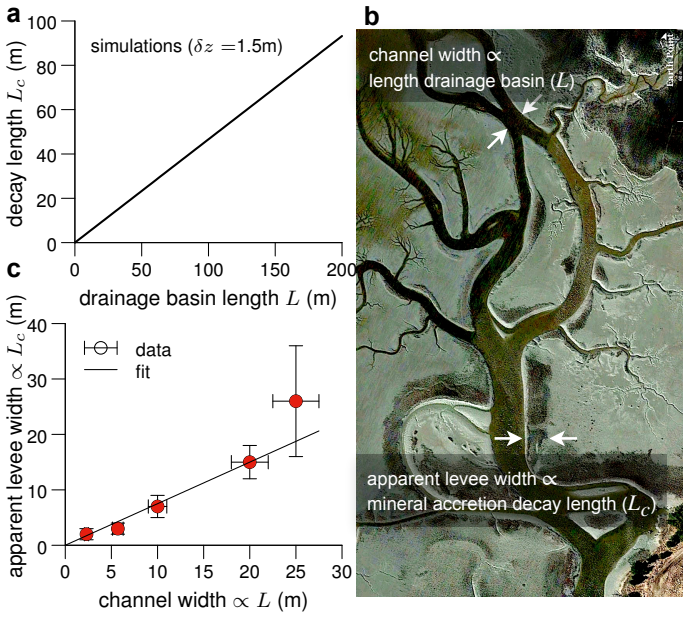


Figure 4: **Scale invariance of inorganic deposition.** (**a**) Scaling of the decay length $L_c$ and the drainage basin length $L$ in the simulations. (**b**) Tidal channel network in Phillips Creek, VA, USA, showing the apparent width of the levees (darker areas surrounding the channels) increasing with channel width, which suggests sediment deposits in a wider region for larger tidal flows. (**c**) Linear scaling obtained from the analysis of (**b**).

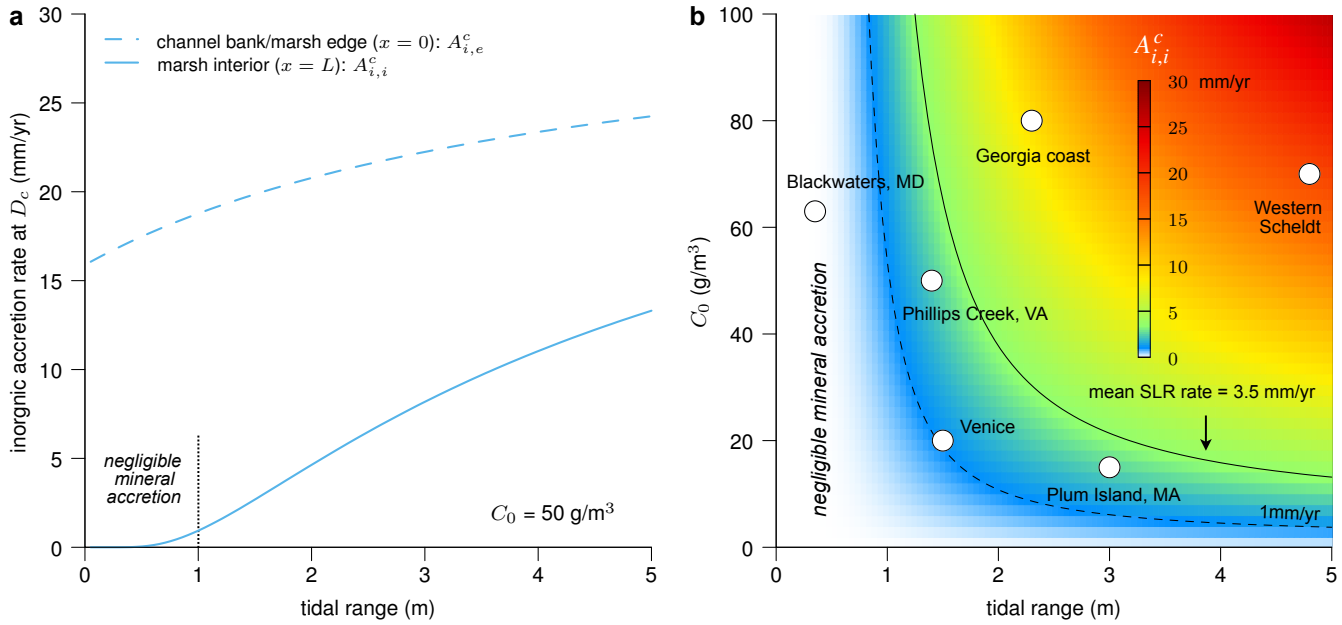


Figure 5: **Predictions of inorganic accretion rates.** (**a**) Inorganic accretion rates at the critical depth $D_c$ evaluated at the marsh edge and marsh interior ($A^c_{i,e}$ and $A^c_{i,i}$, respectively) as function of tidal ranges for an average suspended sediment concentration at the channel bank of $C_0 = 50$g/m$^3$. (**b**) Color scale is the critical inorganic accretion rate at the marsh interior $A^c_{i,i}$ as function of tidal range and average suspended sediment concentration at the channel bank ($C_0$). Black lines separate regions with low inorganic deposition in the marsh interior ($A^c_{i,i} < 1$mm/yr, dashed line) and with inorganic deposition lower than the current global mean rate of SLR ($A^c_{i,i} < 3.5$mm/yr, solid line). Superimposed data: Venice, Italy [3]; Western Scheldt, NL [49]; from USA: Blackwater, MD [31]; Plum Island, MA [36]; Phillips Creek, VA [20]; Georgia, GA [52].

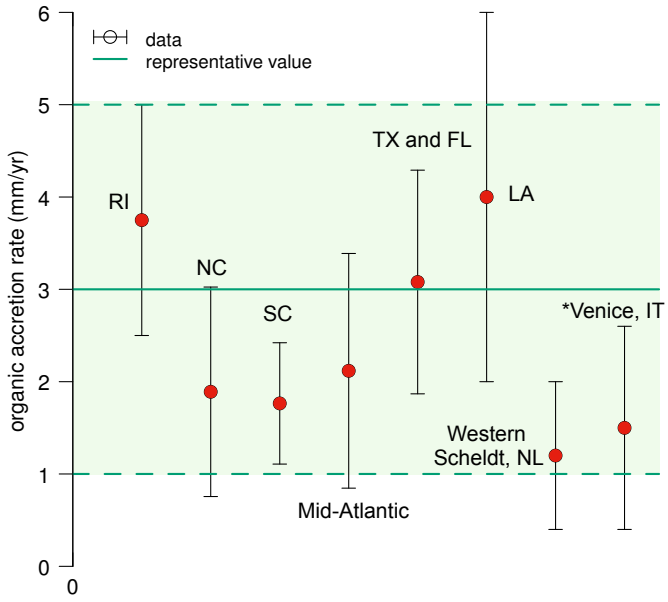


Figure 6: **Range of organic accretion rates.** Organic accretion rates estimated from field data are within $1 - 5$ mm/yr (shadow area). Solid line shows a theoretical maximum for salt marshes [1] (representative value). Field data: Rhodes Island (RI) [50]; North Carolina (NC) [12]; South Carolina (SC) [12]; US Mid-Atlantic average [12]; Texas and Florida (TX & FL) [12]; Louisiana (LA) [46]; Western Scheldt, NL [49]; Venice, Italy (see Methods).

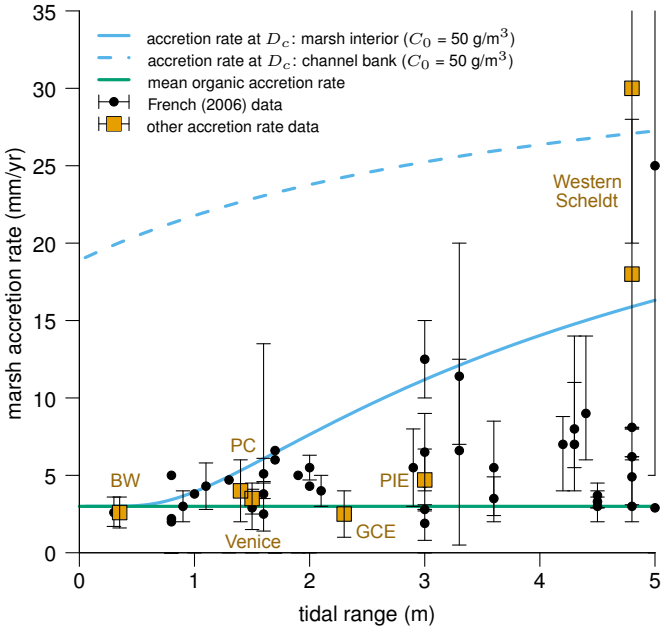


Figure 7: **Comparison of predicted marsh accretion rates to measurements.** Lines are predicted accretion rates at the marsh critical depth ($D_c$) for the marsh edge ($A^c_{i,e} + A^c_o$, dashed line) and marsh interior ($A^c_{i,i} + A^c_o$, solid line) as function of tidal ranges for a typical value of average suspended sediment concentration at the channel bank[44] $C_0 = 50$g/m$^3$. We use a theoretical maximum organic accretion rate for salt marshes[1] $A^c_o = 3$mm/yr (green solid line). Open symbols correspond to the global marsh data compilation in [44]. Filled symbols correspond to: Venice, Italy [51]; Western Scheldt, NL [49]; from USA: Blackwater, MD (BW) [31]; Plum Island, MA (PIE) [36]; Phillips Creek, VA (PC) [53]; Georgia, GA (GCE) [54].

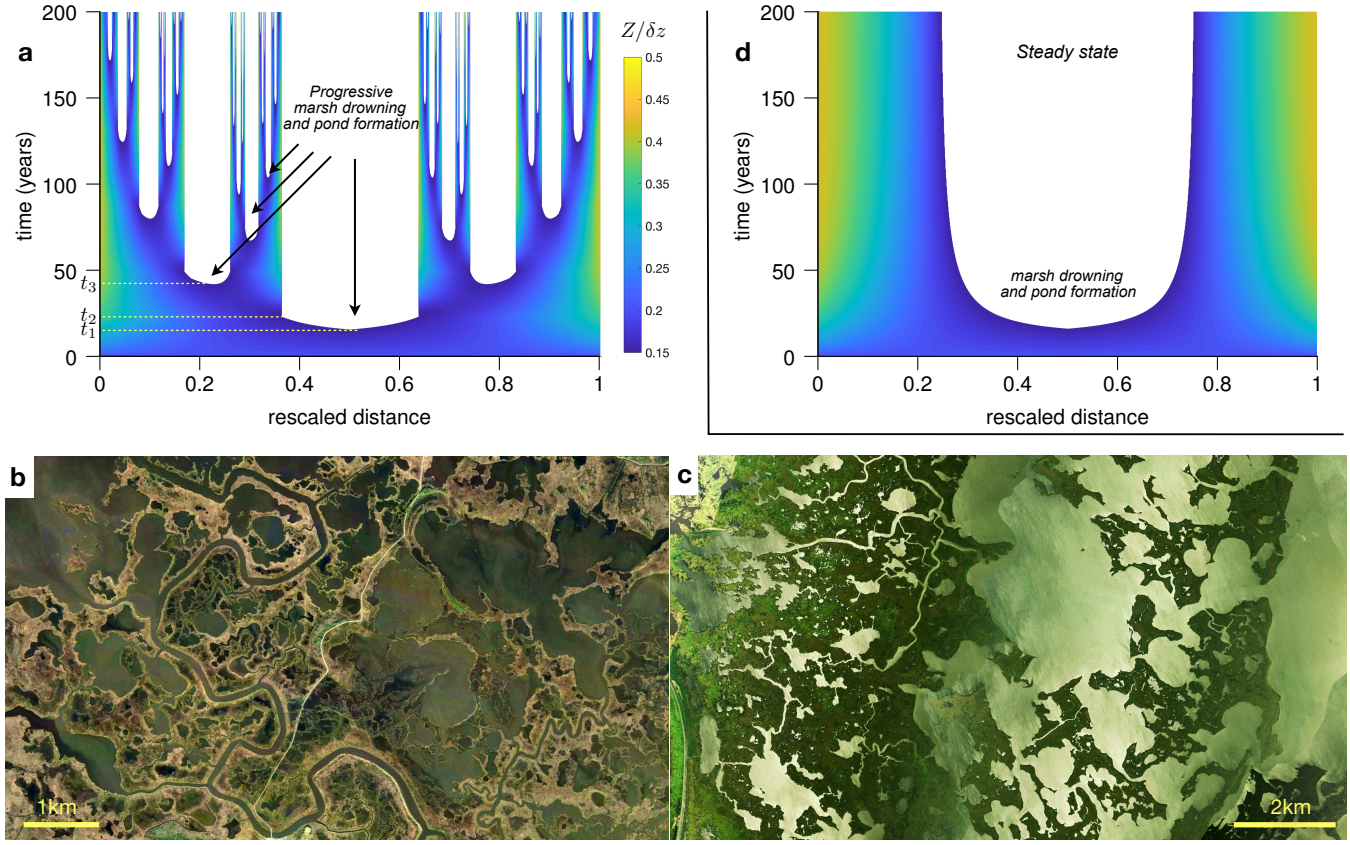


Figure 8: **Self-similar mechanism for marsh drowning.** (**a**) One-dimensional simulation of marsh elevation $Z(x,t)$ (in color) for an interior-marsh drowning scenario (see Methods for description of the model and parameters). White areas represent ponds and/or tidal channels. The self-similar drowning mechanism is as follow: Interior marsh drowning leads to pond formation ($t_1$), ponds expand and eventually connect to the channel network ($t_2$), thus modifying the drainage basin and leading to a new drowning phase ($t_3$). Note the formation of levees around the main channels (at $x = 0$ and $x = 1$) and connected ponds. (**b**-**c**) Examples of apparently self-similar patterns from marshes in Blackwater, MD (**b**) and Louisiana (**c**). (**d**) In the absence of connected ponds, the drainage basin does not change and a new marsh equilibrium is reached.

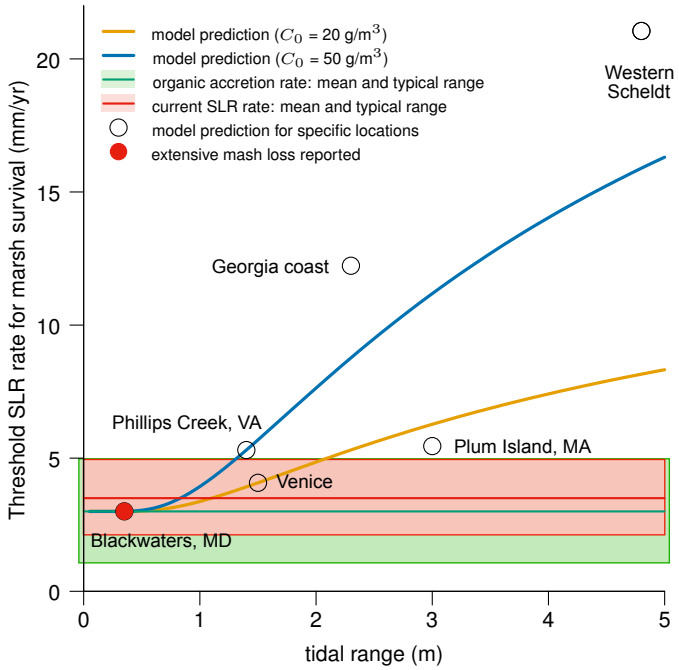


Figure 9: **Threshold rate of SLR for marsh survival.** Lines are predicted thresholds for marsh survival as function of tidal range for two values of the average suspended sediment concentration at the channel bank $C_0$ representing typical low and mid-high sediment supply conditions (see Fig. 5). Symbols represent predictions for specific locations including Blackwater, MD; Plum Island, MA; Phillips Creek, VA and Georgia (we use values shown in Fig. 5b). Current SLR rates in those locations are in the range $3.5 \pm 1.5$mm/yr (red line and region). Organic accretion rates in salt marshes are in the range $3.0 \pm 2$mm/yr (green line and region). See methods for details.